Available online at www.sciencedirect.com

ScienceDirect

journal homepage: www.elsevier.com/locate/he

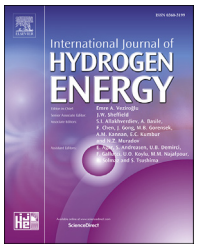

High pressure polymer electrolyte water electrolysis: Test bench development and electrochemical analysis

Michel Suermann [a], *Alexandra Pătru* [a], *Thomas J. Schmidt* [a,b], *Felix N. Büchi* [a,*]

[a] *Electrochemistry Laboratory, Paul Scherrer Institut, CH-5232 Villigen PSI, Switzerland*
[b] *Laboratory of Physical Chemistry, ETH Zürich, CH-8093 Zürich, Switzerland*

ARTICLE INFO

Article history:
Received 16 November 2016
Received in revised form
18 January 2017
Accepted 21 January 2017
Available online 20 April 2017

Keywords:
Polymer electrolyte water electrolysis
High pressure
Electrochemical impedance spectroscopy
High frequency resistance

ABSTRACT

A test bench for a polymer electrolyte water electrolysis (PEWE) cell for high pressure operation of up to 100 bar in differential and balanced pressure mode is described. Important aspects referring to the design, safety and operability of the test bench and the design of a small scale electrolysis cell are described. The electrolyzer cell comprises a special compression mechanism which allows accommodating porous transport layers of different thickness and setting of the compression pressure independent of the clamping pressure. In order to analyze the electrochemical results with respect to the overpotentials, a power source with integrated high frequency resistance (HFR) as well as electrochemical impedance spectroscopy (EIS) measurement capabilities is implemented. The versatility of the test environment is demonstrated by comparing the DC, HFR and EIS data as a function of operating pressure, temperature (up to 70 °C) and current density (up to 4 A/cm^2). With respect to pressurized operation of PEWE cells, only the differential pressure mode (hydrogen pressurized) shows the expected isothermal compression behavior, for balanced pressure operation a different characteristic is observed.

Introduction

Dynamically operable polymer electrolyte water electrolysis (PEWE) is used to store fluctuating electric energy from renewable sources such as wind power and photovoltaics in form of chemical energy by splitting water into hydrogen and oxygen [1,2]. In particular in times when production of electric power exceeds demand, conversion and storage is useful to avoid curtailment [3]. The hydrogen produced, and optionally oxygen, needs to be stored in pressurized gas tanks or caverns or transported in (existing) pipelines. Hydrogen storage pressures of up to 1000 bar are necessary [4], for local storage, transporting the gas or use in mobility. Fuel cells offer an efficient conversion path back to electricity [5] and heat.

Conventionally, mechanical compression is used to compress hydrogen. However, pressurized electrolysis is an alternative to reduce efforts for mechanical compression and gas drying [6]. Furthermore, electrochemical hydrogen compression would seem promising in terms of noiseless hydrogen pressurization with possibly low maintenance [7,8].

* *Corresponding author*. Fax: +41 56 310 2199.
E-mail address: felix.buechi@psi.ch (F.N. Büchi).
http://dx.doi.org/10.1016/j.ijhydene.2017.01.224

Pressurized PEWE can be operated in two different modes: with balanced pressure of hydrogen and oxygen and with differential pressure, with low or ambient pressure at the anode. For differential pressure operation, hydrogen pressures up to 700 bar have been demonstrated [9–12] whichwould be sufficient for direct refueling of today's fuel cell cars. Consistently it was reported that the cell voltage increases with increasing cathodic gas pressure, i.e. the isothermal compression work increases the cell voltage. This holds also true for electrochemical hydrogen compressors [7,8].

For balanced pressures however, operation up to 130 bar without pressure induced change in the cell voltage [13,14] has been reported. Thus the higher thermodynamic cell voltage is compensated by beneficial processes, e.g. increase in oxygen evolution reaction (OER) kinetics [15] and/or better transport properties due to smaller gas volumes as reported earlier by Gregoriev et al. [16] for up to 25 bar.

This work describes a high pressure (differential and balanced, up to 100 bar) PEWE test bench environment, including all necessary safety instrumentation together with the description of a single electrolyzer cell. The test bench is used to characterize the influence of different pressure operation conditions on cell characteristics, using galvanostatic electrochemical impedance spectroscopy (EIS), high frequency resistance (HFR) measurements and DC electrochemical methods.

The aim of this work is to communicate the complexity of a high pressure electrolysis test bench and demonstrate the acquisition of EIS, HFR and DC cell characteristic data for detailed analysis of the overpotential as a function of different operating parameters.

Safety considerations

Obviously, the safety requirements increase with increasing gas pressure, in particular with hydrogen and oxygen. Hydrogen is combustible, especially in close vicinity to oxygen, and pressurized oxygen itself may provoke combustion e.g. with impurities. Further, certain components of the electrolyzer cell are usually made from titanium which in case of high titanium purity, a rough surface and oxygen pressures already in the range of a few bar (which is a function of the (ignition) temperature among other parameters) may lead to self-ignition [17]. However, no incident in PEWE operation attributed to self-ignition has been published so far, which might be due to the presence of liquid water and/or the protective oxide layers on the titanium surface.

Both, for differential and balanced pressure operation, gas crossover through the membrane [18], according to Fick's law, presents a safety issue at high gas pressures. In particular the hydrogen contamination of the oxygen gas needs to be considered as a critical factor, and a combustible atmosphere has to be avoided [19]. The lower explosion limit (LEL) of hydrogen in oxygen is at about 4 mol% under standard conditions, it increases with pressure and slightly decreases with temperature [20].

For the test bench a systematic hazard and operability study (HAZOP) was performed and all failure scenarios from the HAZOP were integrated into the LabVIEW control software. Thus the testing system reacts automatically to safety risk events by different adapted shut down procedures.

Experimental setup

In this section the components of the high pressure test bench are discussed based on the piping and instrumentation diagram (PID) and the schematic cell design. The target specifications to examine the parameters of interest are summarized as follows:

- gas pressures up to 100 bar with a safety factor of three in balanced and differential pressure mode;
- cell temperatures up to 70 °C;
- current densities up to 4 A/cm^2;
- electrochemical characterization (DC, HFR and EIS).

Test bench

General test-bench description: The overall layout of the test bench is shown in the PID in Fig. 1. It consists of one water/gas loop each for oxygen (blue color, component labeling start with 2.) and for hydrogen (red, labeling with 3.) as well as a linking and auxiliary labeling for DC and start/stop procedures (black, labeling with 1.). The components are classified as valves (V), instruments (I) and equipment (E), whereas necessary components for PEWE operation are green bordered, orange are for lifetime and operability issues and black are for safety or auxiliary components. Stainless steel (type 1.4404) is used for the piping.

Water/gas loops: At the anode side deionized water (<1 μS cm^{-1}) is fed by a dosing pump (E-1.2, FLUSYS GmbH, DE) for the entire pressure range. In the anode loop, water is recirculated by a diaphragm pump (E-2.1, LEWA GmbH, DE) with a defined water flow up to 120 mL/min. The cathode loop is based on natural circulation.

Due to the inherently corrosive behavior of the deionized water, especially at temperatures above 60 °C, ions dissolve and accumulate in the water loops and might accelerate degradation processes in the cell. Therefore, an in-house designed ion exchanger is used in the anode loop (E-2.4). Due to expected reduced lifetime of the mixed ion resin bed (LEWATIT® MonoPlus S 108 H and MP 62, Chemia Brugg, CH) at temperatures above 70 °C, this unit requires operation at defined temperatures. If desired, an ion exchanger could be implemented at the cathode too, which however would require a second pump head for the diaphragm pump to ensure recirculation and to overcome the increased flow resistance with the additional benefit of a simplified heat management, as both sides of the cell could be heated or cooled in a defined manner.

On both sides the gases produced are separated from the excess water (anode) and electro-osmotic drag water (cathode) in gas/liquid separators (E-2.0/3.0, SITEC-Sieber Engineering AG, CH) using the density difference. Impedance sensors (I-2.5/3.5, Aquasant Messtechnik AG, CH) are used to control the water levels. Based on the level sensor feedback, on the oxygen side the inlet pump (E-1.2) and on the hydrogen

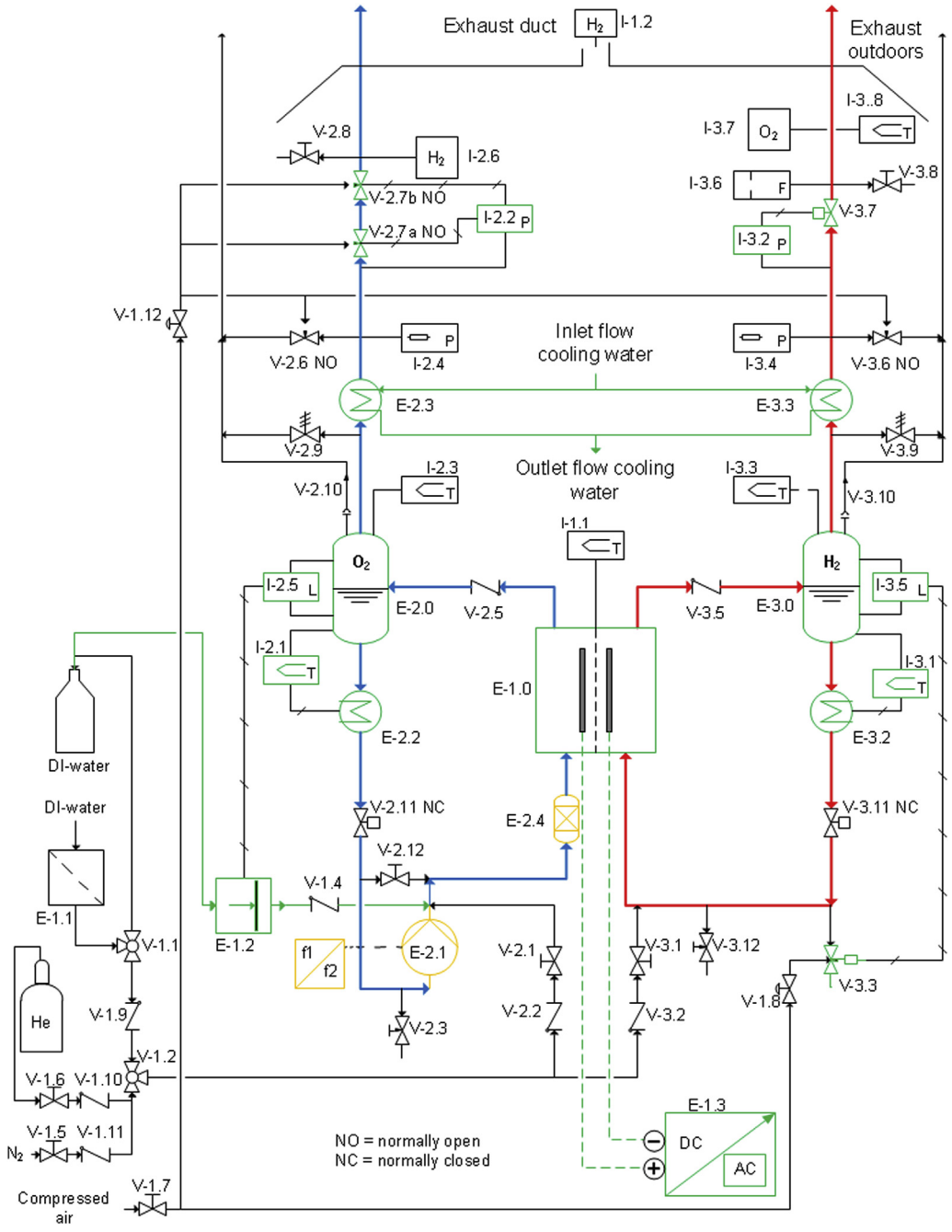

Fig. 1 – Piping and instrumentation diagram of the 100 bar water electrolysis test bench. Labeled as follows: valves (V), instruments (I) and equipment (E) as well as 1.x for linking and auxiliary components (black lines), 2.x for the oxygen path (blue lines) and 3.x for the hydrogen path (red lines). (For interpretation of the references to color in this figure legend, the reader is referred to the web version of this article.)

side the outlet valve (V-3.3) are controlled. Feeding the excess water back to the anode is not realized to avoid any additional contamination of the anode loop [19].

The produced gases are cooled to about 10 °C with tap water in a counter-flow heat exchanger (E-2.3/3.3) for condensing water vapor before exhausting. The operating pressure for the two gases is controlled separately (I-2.2/3.2, V-2.7/3.7, Bronkhorst, CH) in order to have full operational freedom with respect to pressurization, i.e. balanced and differential pressure operation. To cope with pressure pulses in the order of up to 1% of the operating pressure induced by the recirculation pump at the anode, an in-house designed pressure control system with two pneumatic valves (SITEC-Sieber Engineering, CH) are used in a "lock" mode having alternating openings. The volume between the two valves amounts to about 1.5 NmL. That is, a volume determined gas release which is not sensitive to pressure pulses, is implemented instead of a mass flow controlled release.

The components described above are required for operation of a single cell PEWE for pressurized operation; all other components shown in the PID in Fig. 1 are required for safety of operation to comply with the requirements of the HAZOP study. Due to the gas crossover through the membrane or possible membrane failures a hydrogen sensor (I-2.6, BlueSens gas sensor, DE) is integrated in the oxygen exhaust and oxygen is detected in the hydrogen off-stream (I-3.7, GHM Messtechnik, DE). As no gas purity sensors were found able to handle elevated pressures, measurement of the released, unpressurized gas results in a in a small temporal delay of the measurement. To handle possible failures of the pressure control, redundant analog pressure sensors are installed (I-2.4/3.4, Brooks Instrument, US) as well as explosion disks (V-2.10/3.10), overpressure valves (V-2.9/3.9) and pneumatic normally open security valves (V-2.6/3.6, all SITEC-Sieber Engineering, CH) are necessary. For inertisation and leak testing nitrogen and helium is provided. An image of the test bench is shown in Fig. 2.

Electrolyzer cell design

Cell design: The electrolysis single cell (E-1.0) with an active area of 4 cm^2 was designed in-house with support of a specialized company (SITEC-Sieber Engineering, CH) for solving gasket issues. The relatively small size is chosen to suppress gradients along the channel (gas/water ratio, temperature, etc.). This concept is called a differential cell and makes interpretation of measurement data easier, as no gradients in flow direction have to be considered.

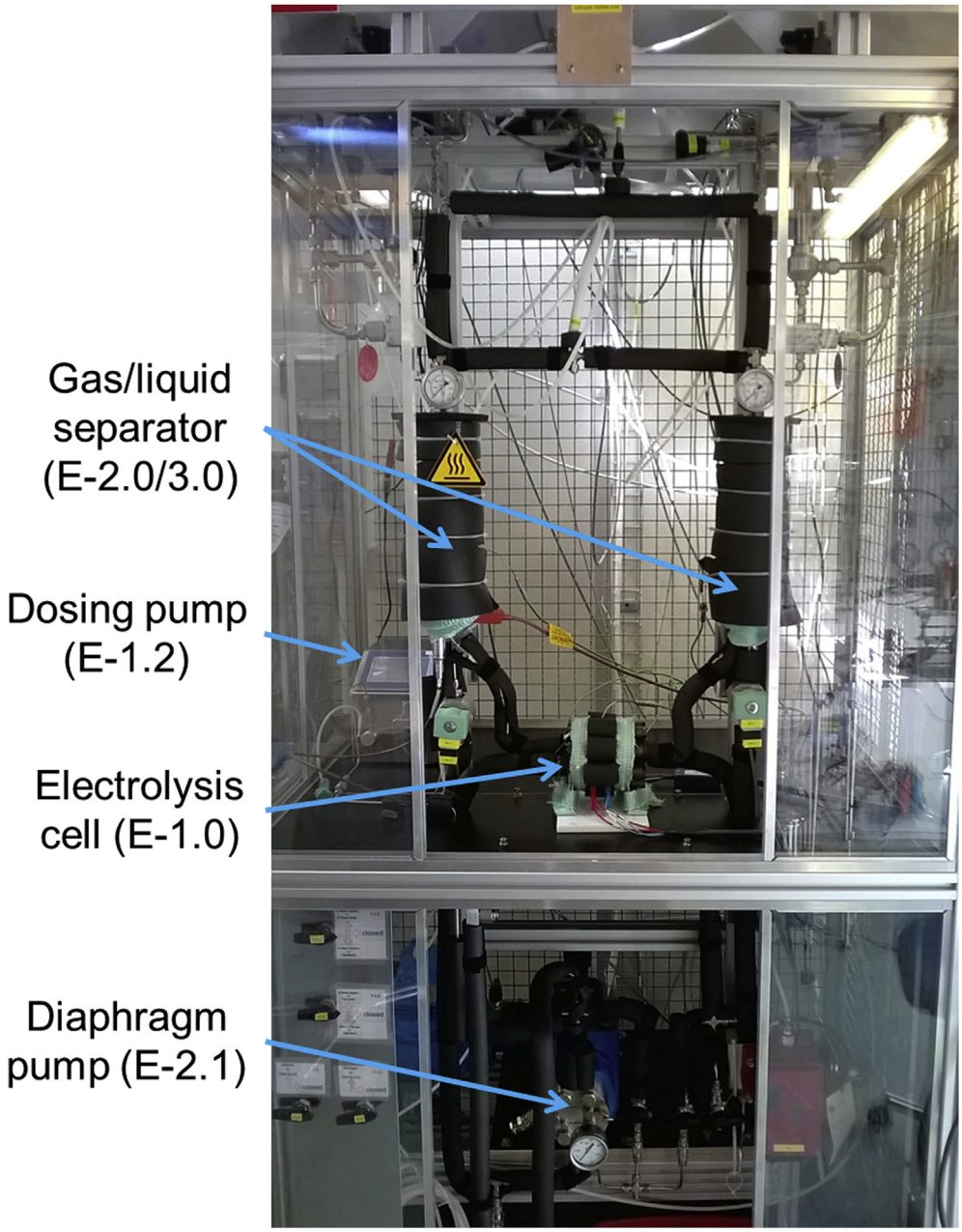

Fig. 2 – 100 bar water electrolysis test bench according to the PID shown in Fig. 1.

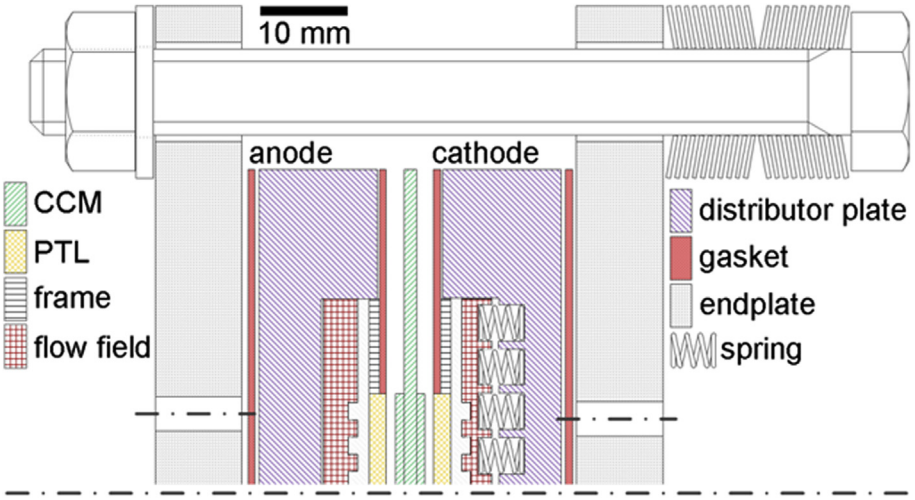

Fig. 3 – Schematic drawing of the high pressure polymer electrolyte water electrolyzer single cell.

The cell construction is schematically shown in Fig. 3. Catalyst (Ir- and Pt-based) coated membranes (CCM, Greenerity® E400, Solvicore, DE, with either Nafion 117CS or Nafion 212 with a wet thickness of about 200 and 64 μm [21,22], respectively) are sandwiched between two porous titanium sintered powder materials (SIKA T series, GKN Sinter Metals Filters, DE) which are used as the porous transport layers (PTLs). Two different materials T5 and T10, having different pore sizes (where the number indicates the maximum particle diameter (in μm) passing the material) with two different thicknesses (1 and 2 mm) are used. In case differential pressure is applied, the anodic PTL mechanically supports the membrane. For water supply and gas removal from the PTL and CCM flow field plates are used, housed in distributor plates which are then compressed by endplates.

Water is fed to the anode through a flow field with 5 straight parallel channels (1 mm height, 2 mm width) separated by 2 mm ribs. An identical flow field structure is used at the cathode. The cell is designed with a mechanism keeping the CCM compression pressure independent of the clamping pressure (high for sealing reasons) using a set of springs supporting the cathode flow field. The adjustable springs permit to set a defined homogeneous contact pressure (0.6–2.6 MPa, results shown here with 2.5 MPa) between flow field, PTL and CCM. In this configuration balanced and differential pressure operation, where the hydrogen pressure exceeds the oxygen pressure (as usually desired) is possible, otherwise the anode and cathode have to be switched.

The flow fields, distributor and end plates (all type 1.4571), the frames (type 1.4404 or 1.4301) and springs (spring steel) are made from stainless steel of different qualities. All steel components which are in contact with deionized water, oxygen and hydrogen are protected by a galvanic coating (10 μm gold on a nickel undercoating, Silbag, CH) to avoid corrosion as well as to ensure a sufficient electrical contact [23].

Gasket: An 80 μm glass fiber reinforced PTFE sheet is used as a flat gasket between the distributor and endplates. The surface roughness of the stainless steel components corresponds to a value of N6. The same gasket material is used as a protective layer between the acidic membrane and the distributor plates to avoid interaction between the acidic membrane and the protective gold coating.

Cell temperature: The cell temperature is measured by a thermocouple (I-1.1) inside a drill hole in the cell housing close to the active area (ca. 13 mm). Since the waste heat production of the single small scale cell in this work is insufficient to reach the desired cell temperature, additional heaters of the feed water (E-2.2/3.2) are implemented to control the cell temperature, whereas the major heat fraction is transferred through the anode due to the forced water recirculation.

An image of the assembled electrolyzer cell, without heat insulation, is shown in Fig. 4.

Leakage rate: The leakage rate of the complete test bench was measured at room temperature over several hours using helium at pressures up to 100 bar and was determined to be in the order of 10^{-4} to 10^{-3} mbar L s^{-1}. The volume of each loop is

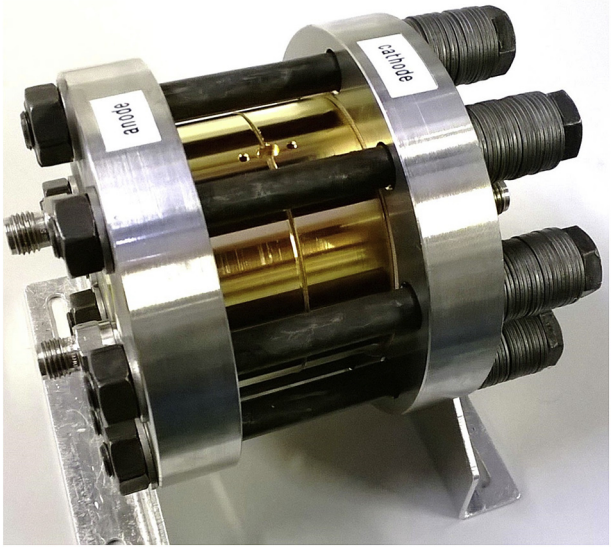

Fig. 4 – High pressure polymer electrolyte water electrolysis single cell (without heat insulation).

about 250 NmL, mainly contained in the gas/liquid separator. The leakage rate of the electrolyzer cell itself was tested separately with no detectable leakage using the applied pressure drop method.

Electrochemical measurement methods

In this work galvanostatic current–voltage characteristics (i/E-curves), high frequency resistance (HFR) and galvanostatic electrochemical impedance spectroscopy (EIS) measurements are reported. All electrochemical measurements were performed using a potentiostat (E-1.3, VSP-300, with two 5 V/10 A booster boards, Z-board, Bio-Logic SAS, FR) fully integrated into the test bench software.

Generally, the cell is operated at 2 A/cm^2 until the desired pressure and temperature (measured with the thermocouple I-1.1) are reached. The current density of 2 A/cm^2 is chosen in terms of safety consideration with respect to gas crossover at high pressures.

For i/E-curves the current density range from 0.001 to 4 A/cm^2 can be measured. Relatively short holding times of 10 s plus 1 s for HFR measurement were chosen. As reported earlier the holding time is a compromise between equilibrium conditions, especially thermal equilibrium, and safety, i.e. gas crossover at low current densities [15]. There are slight deviations from the thermal equilibrium, during i/E-curves because of the large mass of the cell (housing) compared to the small active area. The changes in heat production due to the overpotentials lead to a cooling effect for current densities below and a heating effect for current densities above the reference value (2 A/cm^2). Due to higher overpotentials, this effect is larger for lower cell temperatures, as explained in detail in our previous work [15]. Values given are averages and standard deviation of three measurements.

The HFR (recorded at 25 kHz) is used to determine the ohmic overpotential (η_{iR}). From the HFR measurements of cells with two known membrane thicknesses, the contributions of the electronic and the ionic ohmic overpotential was determined by extrapolating the HFR to a membrane thickness of zero. The cell specific electronic area resistance is about 23 mΩ cm^2 and is independent of temperature and current density; for details see our previous publication [15]. If not mentioned, all presented cell voltages and HFR values are corrected by the cell specific electronic area resistance to ensure a reliable overpotential analysis.

Galvanostatic EIS data were recorded between 100 kHz and 100 mHz with 10 measurement points per decade and with an excitation amplitude of 10% of the applied current. For statistics, the average and standard deviation of three different measurements are presented.

For the EIS data in Fig. 6, recorded for a range of pressures and current densities, to comply with the safety requirements and avoid long measurement times at low current densities and high gas pressures only one measurement per frequency was recorded. Additionally a holding time of 1 min at the reference current density of 2 A/cm^2 was chosen in between each EIS measurement. The impedance spectra were fitted to an equivalent circuit using a combined randomized and simplex algorithm (Software EC-Lab) with 10000 and 5000 iterations, respectively.

Results and discussion

In this section first the results of the electrochemical characterization (DC, HFR and EIS) of the differential cell as a function of balanced and differential pressure, cell temperature as well as current density are presented and discussed with respect to consistency of the different measurement techniques. In the second part the water management due to the electro-osmotic water drag is addressed. In the end, the gas crossover is discussed in terms of safety considerations and linked to the PID and HAZOP introduced in the experimental section.

Electrochemical characterization

Galvanostatic polarization curves and EIS measurements of the PEWE cell with Nafion 117 as the membrane are shown in Fig. 5. In Fig. 5A and B the balanced pressure is varied from 1 to 100 bar at a cell temperature of 50 °C. In Fig. 5C and D the influence of differential pressure is investigated in the range up to 50 bar cathode pressure, again at 50 °C. Here the anode pressure is kept at ambient pressure. Regarding the 50 bar differential pressure experiments, the oxygen exhaust had to be diluted with nitrogen to comply with the safety requirements. In Fig. 5E and F the balanced operating pressure is kept constant at 10 bar and the cell temperature is varied from 30 to 70 °C.

With respect to pressure, an isothermal compression behavior is expected according to the Nernst equation, which defines the thermodynamic cell voltage $E^0(p,T)$, as function of pressure and temperature, as follows:

$$E^0(p,T) = E^0(T) + \frac{R\cdot T}{2\cdot F} ln\left(\frac{a(H_2)\cdot\sqrt{a(O_2)}}{a(H_2O)}\right) \quad (1)$$

with $E^0(T)$ the temperature dependent equilibrium potential [24] and a the activity of the species. For the activity of the gases, ideal gas behavior is assumed [25–27]. The activity of water is assumed as unity.

According to Equation (1) the expected thermodynamic cell voltage increase at 50 °C as function of pressure is 32 and 48 mV/dec for differential and balanced pressure, respectively. For the differential pressure (see Fig. 5C) an isothermal compression behavior close to the theoretical value is observed, For the iR-free cell voltage between 1.4 and 2.6 A/cm^2, for 10 and 50 bar differential pressure, +25 ± 1 mV and +52 ± 2 mV, respectively are measured (theoretical values 32 and 54 mV). For balanced pressure of 1, 10 and 100 bar however, at relevant current densities above about 1 A/cm^2, the (iR-free) cell voltage shows no clear trend and seems to be rather pressure independent within the standard deviation of the measurement (see Fig. 5A).

Increasing the temperature from 30 to 70 °C reduces the cell voltage at a given current density. For instance, at 2 A/cm^2 the cell voltage and the iR-free cell voltage (given in brackets) drop from 2.52 (1.95), to 2.28 (1.85) and 2.13 V (1.78 V) when increasing the cell temperature from 30 to 50 and 70 °C, respectively. With the relatively thick Nafion 117 membrane, with a swollen thickness of about 200 μm [21], as expected a large performance gain is attributed to the ohmic

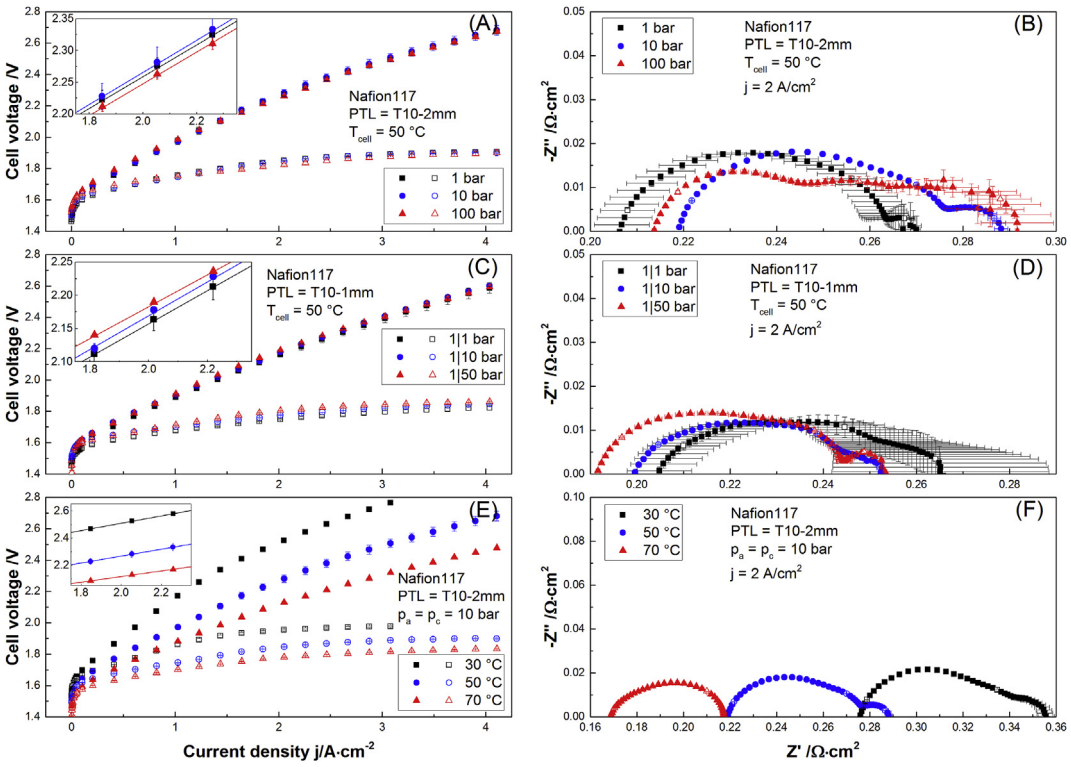

Fig. 5 – Galvanostatic i/E-curves and EIS measurement data for variation of (A&B) balanced pressure, (C&D) differential pressure and (E&F) temperature, at balanced pressure of 10 bar; in i/E-curves the filled symbols represent the cell voltage, the open symbols the iR-free cell voltage; EIS spectra were recorded at 2 A/cm² for all conditions; in the Nyquist plots the frequencies 10 kHz, 100 Hz and 1 Hz are marked with open symbols. All experiments were performed with Nafion 117 based CCMs and the PTLs indicated in the plots.

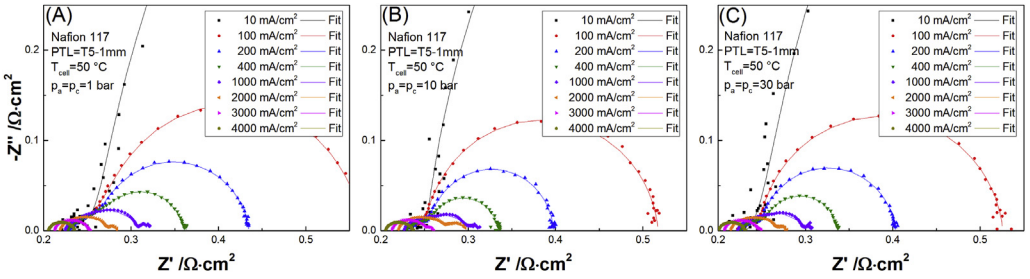

Fig. 6 – EIS data (symbols) as a function of the balanced pressure (1, 10 and 30 bar, as indicated in the plots) and current density; lines represent the fit using the electrical equivalent circuit shown in Fig. 7; in this data the cell specific electronic area resistance is included.

overpotential. The area resistance, obtained from the HFR intercept at frequencies at 25 kHz, drops by 38% from 0.275 (30 °C) to 0.170 Ω cm² (70 °C), so 47% of the voltage gain at 2 A/cm² in this temperature range is due to reduced membrane resistance. In contrast, only relatively small differences in the HFR intercept at 2 A/cm² with pressure, in the range of ±5%, are observed (see Fig. 5B and D) which are referred to experimental inaccuracies. The corresponding EIS data is summarized in Table 1.

For the galvanostatic EIS measurements, typically two semicircles are observed. This is independent of the current density (see Fig. 6), differential and balanced pressure and temperature (Fig. 5), except for the 70 °C cell temperature where the two arcs overlap.

To show the integrity of the test bench, the small scale electrolyzer cell and the measurement system, the low frequency resistance (LFR) intercept and the corresponding slope of the polarization curve are compared in Table 1. For all EIS measurements, performed at 2 A/cm², the LFR intercept is recorded at around 1 Hz. The corresponding slope of the polarization curves is derived by using a linear fit between 1.6 and 2.4 A/cm², as highlighted in the insets of Fig. 5A, C and E. The LFR and the corresponding i/E-curve slope values coincide within ± 15% for all measurements, except for the 30 °C cell

Table 1 – Comparison of the slope of the i/E-curves between 1.6 and 2.4 A cm^{-2} with the low frequency resistance intercept of the EIS data; high frequency intercept shown as membrane resistance data; all EIS measurements were performed at 2 A cm^{-2}; pressure values are given in absolute pressures.

Cell temperature T_{cell} °C	Anode pressure p_a bar	Cathode pressure p_c bar	Slope i/E curve Ω·cm^2	Low frequency resistance (LFR) intercept Ω·cm^2	High frequency resistance (HFR) intercept Ω·cm^2
50	1	1	0.25	0.27	0.21
	10	10	0.25	0.29	0.22
	100	100	0.25	0.29	0.21
50	1	1	0.25	0.26	0.21
	1	10	0.25	0.25	0.20
	1	50	0.24	0.25	0.19
30	10	10	0.27	0.36	0.28
50			0.25	0.29	0.22
70			0.21	0.22	0.17

temperature. The decreasing congruence of the slope of the i/E-curve and the LFR intercept with decreasing cell temperature can be explained by the slightly non-isothermal behavior of the i/E-curves at the current densities different from the reference current density (2 A/cm^2) as discussed in the experimental section and in detail in previous work [15]. Nevertheless, this underlines the accuracy and reproducibility of test cell and measurement set-up.

Commonly impedance spectra are further investigated by fitting to an electrical equivalent circuit. Thus the observed thermodynamically unexpected behavior of the balanced pressure (Fig. 5A) is further investigated as discussed below. EIS data were recorded as a function of balanced pressure (up to 30 bar) and as a function of the current density (0.01–4 A/cm^2).

As shown in Fig. 6, the expected dependence of the spectra on current density is observed. At low current densities a relatively small semicircle at high frequencies and a large arc at low frequencies are observed. With increasing current density the low frequencies arc is reduced and tends to merge with the high frequency arc.

The interpretation of the spectra is non-trivial and different interpretations are given in the literature. Some reports refer to the low frequency semicircle as mass transport losses, whose extent increases with increasing gas to water ratio [28] or decreases by increasing the current density [29]. Lettenmeier et al. [30] attribute the high frequency arc with charge transfer processes combined with the charging of the double layer capacitance of the materials and oxides in the active layer.

Nevertheless, the exchange current density for the highly reversible hydrogen evolution reaction (HER) on platinum is higher [31] and its overpotential smaller as compared to the irreversible oxygen evolution reaction (OER) on IrO_2 [32]. Therefore, the semicircle at high frequencies was also related to the cathodic process and consequently the arc at low frequencies to the anodic process [33].

The data presented from Fig. 6 is therefore further analyzed by fitting of the electric equivalent circuit shown in Fig. 7. This circuit is similar to the one proposed in Ref. [30]. The two electrodes are modeled with a parallel connection of a resistance ($R_{2,3}$) and a constant phase ($Q_{2,3}$) element and the membrane as ohmic resistor R_1. The double layer capacitance was approximated by a constant phase element (CPE) to

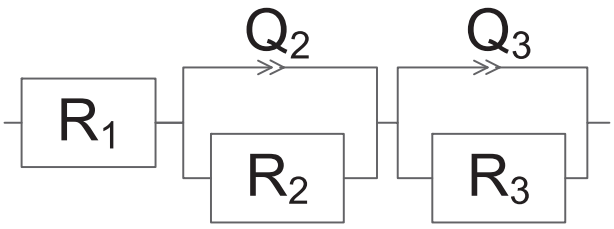

Fig. 7 – Electric equivalent circuit used for fits presented in Fig. 6.

account for the non-ideal behavior of the capacitive elements due to surface heterogeneity (e.g. surface roughness, impurities, etc.). The double layer capacitance C_{DL} is given by the equation:

$$C_{DL} = Q \cdot (\omega)^{a-1} \quad (2)$$

where a is a dimensionless parameter $0 < a < 1$ and $a = 1$ corresponds to an ideal capacitor, Q is a constant with units $F \cdot s^{(a-1)}$ and ω is a frequency (s^{-1}).

As shown in Fig. 8 the resistances R_1, R_2 and R_3 are almost independent of the balanced pressure, but R_2 and R_3 decrease, with increasing current density. The relatively small decline of R_1 can be related to an increase in the actual temperature at the active area/membrane at higher current densities. This is in line with previous findings [15]. The interpretation of the strong decrease of the charge transfer resistances (R_2 and R_3) by up to two orders of magnitude for current densities up to 4 A/cm^2 is based on the fact that with increasing overpotentials from around 0.3 V (10 mA/cm^2) up to around 1.4 V (4 A/cm^2) the charge transfer resistance drops.

With respect to the CPEs, Q_3 seems to be almost independent of pressure and current density, while for Q_2, no distinct trend could be observed, which prevents further interpretation indicating the necessity of further experiments. However, both Q_2 and Q_3, behave close to an ideal capacitor, indicated by the values for a_2 and a_3 being close to 1.

Summarizing, increasing pressure induces thermodynamic cell voltage increases, according to Equation (1). The pressure independent (iR-free) cell voltage, at relevant current densities, for the balanced pressure consequently indicates a change in the overpotentials. However, even with EIS analysis

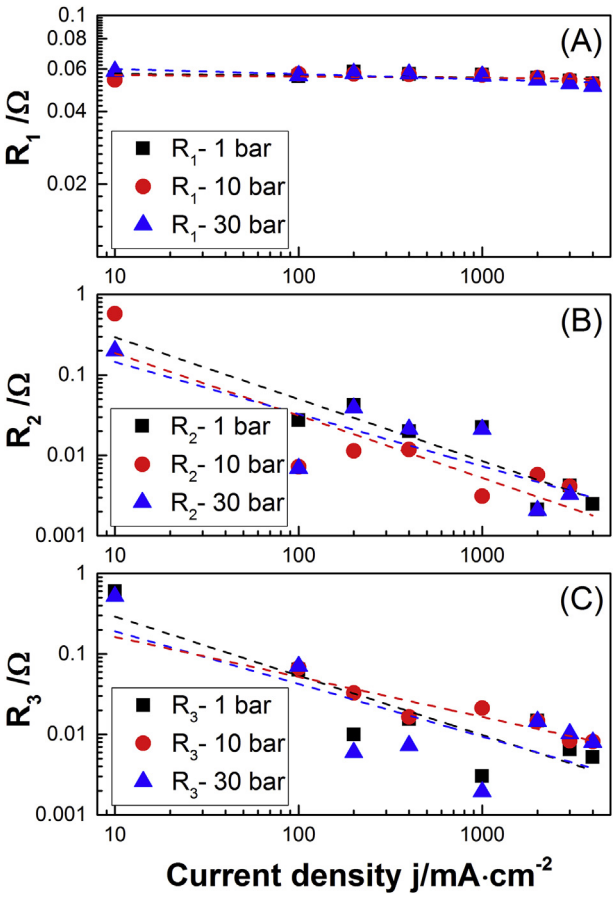

Fig. 8 – Results of the impedance analysis using the equivalent circuit shown in Fig. 7, data are plotted double-logarithmically; linear fits are added to underline trends with current density; data is taken from Fig. 6 with the cell specific electronic area resistance included.

no clear trend was observed for the fitted values with the equivalent circuit used. The reasons are not clear at this time and the necessity for additional studies is emphasized. The relatively small difference in the thermodynamic cell voltage of about 48 mV per decade of pressure (at 50 °C) may be superimposed by the relatively large change of the overall overpotential, which is in the order of hundreds of mV.

Electro-osmotic water drag

With respect to the water management of electrolysis cells, the electro-osmotic water drag has to be considered. On the one hand more water than needed for the water splitting reaction has to be supplied. And on the other hand water which is transported from the anode to the cathode has to be released or recycled. The electro-osmotic drag coefficient (n_{eo}) is defined as the ratio of moles of water per moles of protons transported from the anode to the cathode.

With the water separators, equipped with water level sensors (I-3.5, see PID in Fig. 1), the electro-osmotic drag can be measured accurately. When the cathodic water level is kept constant, the net drag coefficient ($n_{eo,net}$) i.e. the water leaving the cathode, can therefore be determined by measuring the released excess water (through V-3.3, see PID in Fig. 1) over a defined time. The net drag coefficient was determined for a range of temperatures (30–70 °C), balanced pressures (1–70 bar), differential pressures up to 10 bar and current densities between 1 and 3 A/cm^2.

Contrary to the results from Medina et al. [11] who reported a dependence of the drag on current density (up to 1 A/cm^2) and differential pressure (up to 70 bar) and no dependence with respect to the cell temperature, the present measurements show a dependence mainly on the cell temperature, as shown in Fig. 9. The net drag coefficient $n_{eo,net}$ increases from 2.6 to 3.3 H_2O/H^+ from 30 to 70 °C ($n_{eo,net}$ = 0.0182*T [K]–3.0). No clear trend can be identified for the other investigated parameters. An average value of 2.7 ± 0.2 H_2O/H^+ is observed for all the measurements at 50 °C.

The measured temperature dependence is qualitatively in line with results from Onda et al. [34], even if their data suggest a slightly higher net drag of 4.1–4.6 mol(H_2O)/mol(H^+) in the same temperature range ($n_{eo,net}$ = 0.0134*T [K] + 0.03). With respect to the influence of high differential pressures, hydraulic permeability through the membrane could be expected to lead to a lower net drag. However the relatively low hydraulic permeability of Nafion needs to be considered [35], validating present data with no significant measurable influence of the differential pressure.

Gas crossover and safety

As mentioned above, one of the main challenges in high pressure PEWE is related to the gas crossover. On the one hand the gas crossover has to be considered in terms of gas purity and safety [19], on the other hand it lowers the faradaic efficiency of the PEWE system.

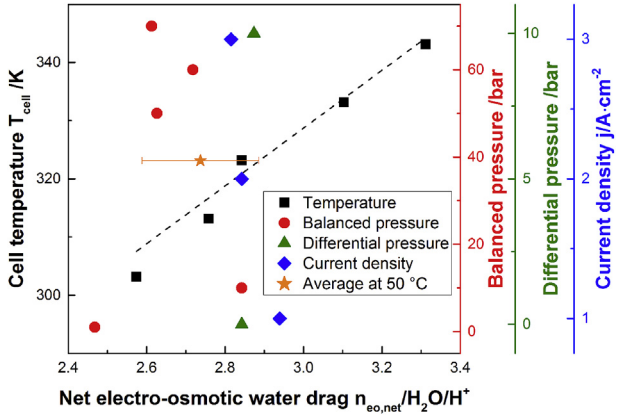

Fig. 9 – Net electro-osmotic water drag coefficient vs. cell temperature for cells with Nafion 117 at 2 A/cm^2, 10 bar balanced and 50 °C (left y-axis, black squares for data points, dashed line for linear fit); influence of balanced and differential pressures as well as current density (right y-axis, red, green and blue symbols); for the differential pressure data the anode pressure is at atmospheric pressure. (For interpretation of the references to color in this figure legend, the reader is referred to the web version of this article.)

According to Schalenbach et al. [18] and Sakai et al. [36] the gas permeability for PFSA membranes (e.g. Nafion) increases by about one order of magnitude from the fully dry to the wet state, i.e. the membrane equilibrated in liquid water. Additionally for wet Nafion, for a temperature increase from 40 to 80 °C the gas permeability increases about threefold [18,36]. When defining the hydrogen gas cross-over current density equivalent as $j_{x,H2} = 2F^*(P_{H2}/\delta)$ where F is the Faraday constant, P the permeability and δ the membrane thickness, then with reported values for the hydrogen permeability of wet Nafion at 55 °C of $3.16 \cdot 10^{-11}$ mol cm^{-1} s^{-1} bar^{-1} [18], $j_{x,H2}$ corresponds to about 0.3 mA cm^{-2} bar^{-1} for Nafion 117. The oxygen crossover is around half of that of the hydrogen crossover [18,36].

In the presented setup both contaminating gases are measured in the exhaust pipelines (I-2.6, I-3.7, see PID in Fig. 1). However, at the cathode the platinum based catalyst promotes the recombination of hydrogen and oxygen back to water. With the employed oxygen sensor, with the warranted measuring range starting at 0.1%, no oxygen was detected in the hydrogen exhaust even at 100 bar balanced pressure. Contrary, at the anode the hydrogen in oxygen contamination is determined to about 3.0± 0.4% H_2 in O_2 at 100 bar, measured for four different cells with Nafion 117 at 2 A/cm^2 and 50 °C cell temperature.

To cross-check the validity of the measured values, the hydrogen fraction in oxygen can be calculated as follows:

$$H_2\% \text{ in } O_2 = \frac{j_{x,H_2} \cdot p_{H_2}}{0.5 \cdot j - j_{x,H_2} \cdot p_{H_2}} \quad (3)$$

where $j_{x,H2}$ is the hydrogen gas crossover current density equivalent, p_{H2} the hydrogen (partial) pressure and j the applied current density. At a current density of 2 A/cm^2, the oxygen gas crossover current density equivalent is relatively small and thus neglected in Equation (3). Using Equation (3) the calculated percentage of H_2 in O_2 is 3.1% which matches well with the measured value of 3.0 ± 0.4% and underlines again the versatility of the set-up and Fickian behavior of the hydrogen crossover, at least for balanced pressure operation.

Conclusions

In this study, both the complexity in terms of engineering, operability and safety as well as electrochemical diagnostic methods based on DC, HFR and EIS for a high pressure polymer electrolyte water electrolysis test environment are reported.

Based on the piping and instrumentation diagram the safety requirements for gas pressures up to 100 bar are outlined. Both the pressure itself and the challenges due to the gas crossover are discussed.

Electrochemical measurements are validated by comparing the low frequency intercept of the EIS data with the corresponding slope of polarization curves. A good agreement, independent of the cell temperature, as well as balanced and differential pressures was found. This proves the integrity of the test bench including the differential cell together with the DC, HFR and EIS measurement setups.

With respect to the influence of pressure on cell performance, the differences between differential and balanced pressure operation were compared. With differential pressure operation the expected isothermal compression behavior, i.e. a higher cell voltage, is confirmed. Contrary, for balanced pressure operation only minor influence on the cell voltage was observed at relevant current densities (above 1 A/cm^2) indicating that beneficial processes compensate the thermodynamically expected cell voltage increase. EIS measurements were employed to closer study the different processes, however the nature of the beneficial process(es) of balanced pressure operation could not be identified, probably because the relatively large overpotentials superimpose the small change in the thermodynamic cell voltage and make identification difficult. Further investigations to understand the effects are needed.

Acknowledgments

Funding by the Swiss Federal Office of Energy (SFOE, contract no. SI/500904-01), Belenos Clean Power Holding Ltd. and the Energy System Integration (ESI) platform at PSI, and technical support by Martin Ammann and Thomas Gloor (both PSI) are gratefully acknowledged. TJS thanks the Commission for Technology and Innovation Switzerland and the Swiss Competence Center for Energy Research Heat & Electricity Storage.

REFERENCES

[1] Ursúa A, Gandía LM, Sanchis P. Hydrogen production from water electrolysis: current status and future trends. Proc IEEE 2012;100:410–26.
[2] Millet P, Grigoriev S. Water electrolysis technologies. In: Gandia LM, Arzamendi G, Dieguez PM, editors. Renewable hydrogen technologies: production, purification, storage, applications and safety. Waltham: Elsevier B.V.; 2013. p. 19–41.
[3] Barnhart CJ, Dale M, Brandt AR, Benson SM. The energetic implications of curtailing versus storing solar- and wind-generated electricity. Energy Environ Sci 2013;6:2804–10.
[4] Stefan M. From prototype to serial production – manufacturing hydrogen fuelling stations. In: 20th world hydrogen energy conference. KDJ convention center Gwangju; South Korea;: committee of WHEC2014; 2014. p. 615–22.
[5] Büchi FN, Hofer M, Peter C, Cabalzar UD, Bernard J, Hannesen U, et al. Towards re-electrification of hydrogen obtained from the power-to-gas process by highly efficient H_2/O_2 polymer electrolyte fuel cells. RSC Adv 2014;4:56139–46.
[6] Bensmann B, Hanke-Rauschenbach R, Müller-Syring G, Henel M, Sundmacher K. Optimal configuration and pressure levels of electrolyzer plants in context of power-to-gas applications. Appl Energy 2016;167:107–24.
[7] Bouwman PJ, Konink J, Semerel D, Raymakers L, Koeman M, Dalhuijsen W, et al. Electrochemical hydrogen compression. ECS Trans 2014;64:1009–18.
[8] Grigoriev SA, Shtatniy IG, Millet P, Porembsky VI, Fateev VN. Description and characterization of an electrochemical hydrogen compressor/concentrator based on solid polymer electrolyte technology. Int J Hydrogen Energy 2011;36:4148–55.
[9] Ayers KE, Anderson EB, Capuano CB, Carter BD, Dalton LT, Hanlon G, et al. Research advances towards low cost, high efficiency PEM electrolysis. ECS Trans 2010;33:3–15.
[10] Norman T, Hamdan M. Unitized design for home refueling appliance for hydrogen generation to 5,000 psi. DOE Hydrogen Fuel Cells Program 2012:122–5.

[11] Medina P, Santarelli M. Analysis of water transport in a high pressure PEM electrolyzer. Int J Hydrogen Energy 2010;35:5173–86.
[12] Ishikawa H, Haryu E, Kawasaki N, Daimon H. Development of 70 MPa differential-pressure water electrolysis stack. Honda R&D Technical Review. 2016. p. 28.
[13] Millet P, Dragoe D, Grigoriev S, Fateev V, Etievant C. GenHyPEM: a research program on PEM water electrolysis supported by the European commission. Int J Hydrogen Energy 2009;34:4974–82.
[14] Grigoriev SA, Porembskiy VI, Korobtsev SV, Fateev VN, Auprêtre F, Millet P. High-pressure PEM water electrolysis and corresponding safety issues. Int J Hydrogen Energy 2011;36:2721–8.
[15] Suermann M, Schmidt TJ, Büchi FN. Cell performance determining parameters in high pressure water electrolysis. Electrochimica Acta 2016;211:989–97.
[16] Grigoriev SA, Khaliullin MM, Kuleshov NV, Fateev VN. Electrolysis of water in a system with a solid polymer electrolyte at elevated pressure. Russ J Electrochem 2001;37:819–22.
[17] Bolobov VI. Mechanism of self-ignition of titanium alloys in oxygen. Combust Explos Shock Waves 2002;38:639–45.
[18] Schalenbach M, Hoefner T, Paciok P, Carmo M, Lueke W, Stolten D. Gas permeation through nafion. Part 1: measurements. J Phys Chem C 2015;119:25145–55.
[19] Grigoriev SA, Millet P, Korobtsev SV, Porembskiy VI, Pepic M, Etievant C, et al. Hydrogen safety aspects related to high-pressure polymer electrolyte membrane water electrolysis. Int J Hydrogen Energy 2009;34:5986–91.
[20] Schröder V, Emonts B, Janssen H, Schulze H-P. Explosionsgrenzen von Wasserstoff-Sauerstoff-Gemischen bei Drücken bis 200 bar. Chem Ing Tech 2003;75:914–8.
[21] Büchi FN, Scherer GG. In-situ resistance measurements of Nafion 117 membranes in polymer electrolyte fuel cells. J Electroanal Chem 1996;404:37–43.
[22] Gubler L, Bonorand L. Radiation grafted membranes for fuel cells: strategies to compete with PFSA membranes. ECS Trans 2013;58:149–62.
[23] Engel RA, Chapman GS, Chamberlin CE, Lehman PA. Development of a high pressure PEM electrolyzer enabling seasonal storage of renewable energy. In: 15th annual US hydrogen conference and hydrogen expo; 2004.
[24] Barin I, Platzki G. Thermochemical data of pure substances. Weinheim: VCH Verlagsgesellschaft mbH; 1995. p. 795–6.
[25] Ito H, Maeda T, Nakano A, Takenaka H. Properties of Nafion membranes under PEM water electrolysis conditions. Int J Hydrogen Energy 2011;36:10527–40.
[26] Wiebe R, Gaddy VL. The solubility oh hydrogen in water at 0, 50, 75 and 100° from 25 to 1000 atmospheres. J Am Chem Soc 1934;56:76–9.
[27] Tromans D. Temperature and pressure dependent solubility of oxygen in water: a thermodynamic analysis. Hydrometallurgy 1998;48:327–42.
[28] Siracusano S, Baglio V, Briguglio N, Brunaccini G, Di Blasi A, Stassi A, et al. An electrochemical study of a PEM stack for water electrolysis. Int J Hydrogen Energy 2012;37:1939–46.
[29] Dedigama I, Angeli P, Ayers K, Robinson JB, Shearing PR, Tsaoulidis D, et al. In situ diagnostic techniques for characterisation of polymer electrolyte membrane water electrolysers – flow visualisation and electrochemical impedance spectroscopy. Int J Hydrogen Energy 2014;39:4468–82.
[30] Lettenmeier P, Wang R, Abouatallah R, Helmly S, Morawietz T, Hiesgen R, et al. Durable membrane electrode assemblies for proton exchange membrane electrolyzer systems operating at high current densities. Electrochimica Acta 2016;210:502–11.
[31] Durst J, Siebel A, Simon C, Hasché F, Herranz J, Gasteiger HA. New insights into the electrochemical hydrogen oxidation and evolution reaction mechanism. Energy Environ Sci 2014;7:2255.
[32] Brightman E, Dodwell J, van Dijk N, Hinds G. In situ characterisation of PEM water electrolysers using a novel reference electrode. Electrochem Commun 2015;52:1–4.
[33] Rozain C, Millet P. Electrochemical characterization of polymer electrolyte membrane water electrolysis cells. Electrochimica Acta 2014;131:160–7.
[34] Onda K, Murakami T, Hikosaka T, Kobayashi M, Notu R, Ito K. Performance analysis of polymer-electrolyte water electrolysis cell at a small-unit test cell and performance prediction of large stacked cell. J Electrochem Soc 2002;149:A1069.
[35] Evans CE, Noble RD, Nazeri-Thompson S, Nazeri B, Koval CA. Role of conditioning on water uptake and hydraulic permeability of Nafion® membranes. J Membr Sci 2006;279:521–8.
[36] Sakai T, Takenaka H, Wakabayashi N, Kawami Y, Torikai E. Gas permeation properties of solid polymer electrolyte (SPE) membranes. J Electrochem Soc 1985;132:1328–32.